On the Characteristics of a Twin-Jet STOVL Fountain

A. J. Saddington*, K. Knowles† and P. M. Cabrita‡

Aeromechnaical Systems Group
Cranfield University
Shrivenham, Wiltshire, SN6 8LA, UK

Abstract

The interaction of multiple jets with the ground is of great importance for the design and operation of short take-off, vertical landing aircraft. The fountain upwash flow, generated by the impingement of two axisymmetric, compressible, turbulent jets onto a ground plane was studied using laser-based particle image velocimetry and laser Doppler velocimetry. Measurements were made with nozzle pressure ratios of between 1.05 and 4, nozzle height-to-diameter ratios of between 2.4 and 8.4, nozzle splay angles of between ± 15 degrees and a nozzle spacing-to-diameter ratio of seven. The effect of varying these parameters on the fountain velocity decay, spreading rate and momentum flux ratio are discussed. Mean fountain upwash velocity profiles were found to be self-similar for all test conditions. A distinct frequency of fountain oscillation was identified but only at a nozzle height of 4.4 diameters.

Nomenclature

a_1	growth rate of fountain half-width
a_2	constant
D	nozzle exit internal diameter
H	nozzle exit height above the ground plane
J	downstream proportion of jet momentum
L	distance between jets' stagnation points
LIC	line integral convolution
$\dot{M}$	fountain vertical momentum flux
$\dot{M}_{\max}$	maximum fountain vertical momentum flux
r	radial distance from nozzle axis
R_f	radial distance from the fountain virtual origin
S	distance between the nozzle centres
u	instantaneous streamwise velocity
U	time-mean streamwise velocity
$\hat{U}$	time-mean peak streamwise velocity
U_j	time-mean jet centreline velocity at nozzle exit
$U_{\max}$	time-mean local maximum streamwise velocity
v	instantaneous velocity in the x-direction
x	co-ordinate in the plane of the jet centres
$x_{0.5}$	fountain half-width
x_1	fountain width
y	co-ordinate in the plane of the fountain axis
z	co-ordinate normal to the ground plane
α	nozzle splay angle (positive outwards)
ϕ	jet spreading half-angle
$\lambda_{\dot{M}}$	fountain momentum flux ratio ($\dot{M}/\dot{M}_{\max}$)
θ	fountain included angle in the y-z plane
ρ	air density

1 Introduction

The wall jets created by the impingement on the ground of the individual jet flows from a jet-lift, short take-off and vertical landing (STOVL) aircraft, with two nozzles, meet at a stagnation line and form an upwards-flowing 'fountain' that interacts with the airframe (Fig. 1). In some cases this can provide a beneficial, lift-generating, effect. The fountain flow may also give rise to a variety of undesirable characteristics: hot gas ingestion; ground erosion; acoustic, thermal and pressure loads on the airframe [1]. Despite many years of STOVL aircraft development, the unsteady nature of in-ground-effect aerodynamics remains poorly understood and continues to be of concern.

Early experimental work on fountain flows revealed that the use of a vertical reflection plane is inappropriate due to the interaction between the jets and the fountain [2]. Although the flow is generally symmetrical in the mean, instantaneous velocity fields show a high degree of asymmetry, the presence of large-scale vortical structures and a stagnation region whose location

*Lecturer, Aeromechanical Systems Group.
†Professor, Head of Aeromechanical Systems Group.
‡Research Student, Aeromechanical Systems Group.

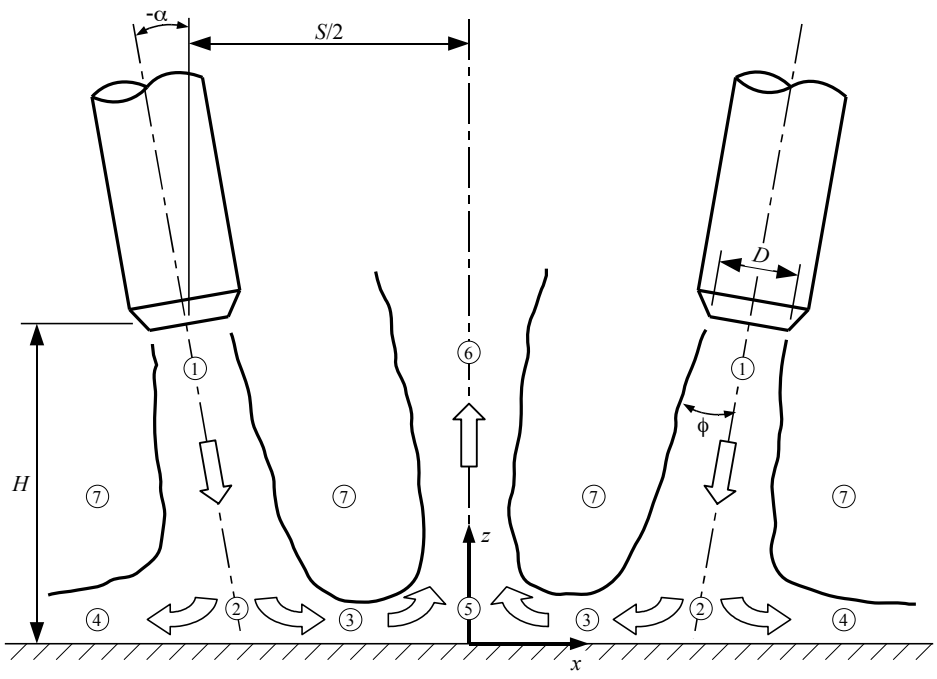

Fig. 1: Schematic of a splayed twin impinging jet fountain flow.

is observed to vary randomly [3]. The fountain is quite sensitive to small imbalances between the jets [4, 5] and appears to be unstable under certain conditions [6]. Further studies have reported turbulence intensities in the fountain upwash as high as 50 per cent and a much greater rate of spreading in the fountain when compared to a free jet [7, 8]. Velocities normal to the axis of the fountain upwash have been found to be in the region of 20 to 30 per cent of the jet exit velocity, at least for incompressible experiments [8, 9]. Positioning of the fountain is largely dependent upon the momentum ratio of the opposing wall jets with differences in their relative thicknesses causing the fountain to appear to lean [10]. Nozzle angle relative to the impingement plane or nozzle splay angle also plays an important part in the fountain location and development [9, 10]. Visualization of multiple jet impingement has revealed the presence of large scale coherent structures, evolving from the main jets, propagating through the wall jets and dissipating in the fountain [11–14], with possible crossover of these structures from one wall jet to the opposite side of the fountain [15]. This may be responsible, in part, for the large degree of spreading associated with fountain flows.

Whilst it is evident that the fountain upwash flow is unsteady, only limited data on the transient characteristics of this flow region are available. Early experiments relied on intrusive measurement techniques to provide mean pressure data [6] with unsteady pressures on the ground plane being used to infer additional information [16]. Early attempts to acquire turbulence data used hot-wire anemometry [7, 17] but this technique is limited to low flow speeds and low turbulence intensities and is therefore inaccurate for compressible and highly unsteady flows. Techniques such as particle image velocimetry (PIV) and laser Doppler velocimetry (LDV) offer the possibility of detailed non-intrusive measurements in the fountain region. Previous investigations using these techniques have used water as the working fluid [8, 9, 18] or were limited to a single nozzle pressure ratio [19]. A combined examination of underexpanded impinging jets and fountain flows is necessary in order to understand the complete effect of NPR (the ratio of nozzle supply total pressure to ambient static pressure) on the development of the fountain.

Rotating the nozzles on the propulsion system of a short take-off, vertical landing (STOVL) aircraft into

a splayed configuration (Fig. 1), and thereby altering the vertical component of thrust, provides a means by which the rate of ascent or descent during vertical flight may be controlled. Such a technique overcomes the inherent lag in the turbomachinery, enabling a more rapid response to control demands, which may be important when operating in close proximity to the ground. Splay may also be used to change the strength of the fountain; splaying the jets away from each other reduces the fountain strength whereas splaying them inwards increases it [1]. If the jets are splayed inwards such that they merge before impingement with the ground then no fountain formation occurs. The ability to schedule splay angle with, for example, aircraft height above the ground, provides the opportunity to trade-off the beneficial lift-enhancing properties of the fountain flow against its detrimental hot gas ingestion and acoustic fatigue characteristics.

Although a significant number of experimental studies have examined the fountain flow generated by parallel impinging jets, far fewer have addressed configurations where the jets are splayed. Notable contributions are included in references [5, 9, 13], however, even these did not focus to any great extent on the effect of splay, regarding it as supplementary to the main investigation of parallel jets. The studies concluded that, in general, outward splay of the jets reduces fountain peak vertical velocity and turbulence intensity. Conversely, inward splay had the opposite effect; fountain vertical velocity and turbulence intensity was increased.

This paper summarizes the findings of a three-year study of the fountain flow-field generated by a pair of round, compressible, turbulent jets impinging onto a flat surface. Nozzle height, pressure ratio and splay angle were varied to determine the effect each has on the fountain flow-field characteristics.

2 Aims and objectives

The continued development of STOVL aircraft, both manned and unmanned, with an increasing reliance on computational design techniques, is dependent upon a better understanding of the aerodynamics of jet-lift aircraft in ground effect. The aim of this work was to describe and quantify the fountain upwash flow-field (generated by a pair of impinging, turbulent, compressible jets) in the plane connecting the nozzle centrelines for a range of geometries and nozzle pressure ratios. The objectives of the work were:

- to gather high-quality PIV and LDV data, which can be used for CFD validation;
- to analyse and quantify the mean flow-field characteristics;
- to analyse and quantify fountain spreading and decay;
- to analyse and quantify any periodic 'flapping' of the fountain flow.

3 Experimentation

Given that the fountain flow has been shown previously to be highly sensitive to small disturbances caused, for example, by probe interference, this study focused on non-intrusive measurements of the flow-field. Such techniques included high-speed digital photography, particle image velocimetry (PIV) and laser Doppler velocimetry (LDV).

3.1 Impinging jet facility

The experiments were conducted in a dedicated impinging jet facility. The test rig (Fig. 2) consisted of a small cylindrical settling chamber with an internal diameter of 230 mm and a height of 210 mm suspended from a 4 m $\times$ 4 m $\times$ 3 m steel frame. This rig was mounted in the centre of a closed room measuring approximately 8 m $\times$ 8 m $\times$ 4 m. The settling chamber has two internal screens and, on the lower surface, a replaceable nozzle-mounting plate that allows different configurations of nozzle spacing and splay angle (Fig. 3). Dried, ambient-temperature compressed air was supplied to the settling chamber through a 63.5 mm diameter flexible hose from two Howden screw-type compressors via a 34 m^3 storage tank. Maximum continuous flow rate was 0.9 kgs^{-1} and maximum pressure was 7 bar(g). The impingement surface consisted of a 1 m $\times$ 1 m aluminium plate placed on top of a 3 m $\times$ 2 m table. The nozzle settling chamber was instrumented with a K-type thermocouple and a Druck PDCR 10-3.5 pressure transducer that provided information on the stagnation temperature and pressure (via the small pressure lines seen in Fig. 2) respectively. Atmospheric pressure was measured using a SETRA 270 pressure transducer. The pressure in the settling chamber was adjusted using a CompAir A119 pneumatically-controlled valve driven by a computer and a current-to-pressure converter. The configuration used for the present study comprised two identical 63.5 mm-long axisymmetric convergent nozzles with an exit diameter, D, of 12.7 mm (following the "short

half-inch" nozzle design used by Bray [20]) and a nozzle spacing, S, of seven diameters. The jets were seeded by JEM Hydrosonic long-lasting fluid droplets ($\approx$1 μm diameter) generated by a TSI 9306 Six-Jet atomizer connected to a Clarke compressor and injected through eight ports in the settling chamber (the large pressure lines seen in Fig. 2). The ambient air was seeded with smoke particles produced by a Le Maitre Turbo Mist fog generator. The uncertainty in the pressure control system was estimated to be $\pm$0.5 per cent of NPR [21].

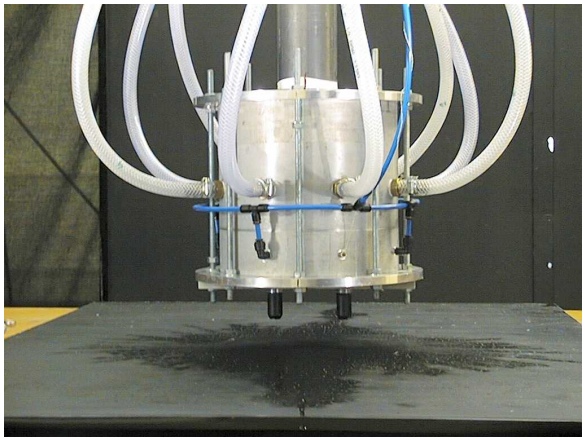

Fig. 2: The settling chamber and impingement surface.

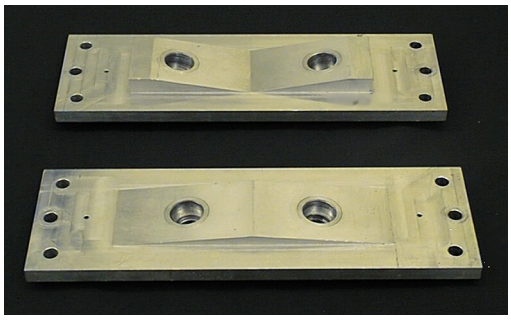

Fig. 3: Splayed nozzle plates: negative (inward) splay, top; positive (outward) splay, bottom.

3.2 Flow visualization

The high-speed flow visualization system consisted of a pulsed laser, a high-speed digital camera, and an atomizer. A Photonics Industries GM-30E Nd:YLF lamp-pumped laser operating in Q-switch mode, combined with one planar concave and one cylindrical lens, generated a light sheet $\approx$1 mm thick and 200 mm high. The laser was synchronized to a Roper Scientific FastCam Super 10k high-speed camera, fitted with an f1.8 Pentax lens of 25 mm focal length, using a TTL pulse for the trigger. It was necessary to include a delay in the TTL pulse to allow time for the camera shutter to open and this was provided by a TTi TGP110 pulse delayer. Images were acquired at a frequency of 1 kHz and a resolution of 256 $\times$ 240 pixels. Images were acquired for height-to-nozzle-diameter ratios, (H/D), of 2.4, 4.4, 6.4 and 8.4, spacing-to-nozzle-diameter ratios, (S/D), of seven, and a nozzle pressure ratio (NPR) of 1.05. Despite the high laser power and high seeding volume, insufficient light was reflected by the seeding particles to enable the satisfactory acquisition of imagery at higher pressure ratios.

3.3 Particle image velocimetry

The PIV equipment consisted of a New Wave Gemini II Nd:YAG double-pulsed laser which, through the use of a combination of plano-concave and plano-cylindrical lenses, created a light sheet approximately 1 mm thick, positioned perpendicular to the impingement plane and passing through the plane defined by the nozzle axes. The PIV double-pulsed image pairs were acquired using a Kodak Megaplus ES1.0 digital camera with a resolution of 1016×1008 pixels at a rate of 15 image pairs per second. The camera was fitted with a 60 mm, f2.8 Nikon lens and placed normal to the light sheet at a distance of approximately 550 mm. This provided a maximum field of view of 82 mm $\times$ 83 mm ($6.4D \times 6.5D$). It was assumed that the maximum velocity in the upwash fountain was around half the maximum jet velocity (assuming isentropic conditions), and the maximum out-of-plane velocity was 25 per cent of the fountain upwash velocity. This resulted in a pulse separation of between 2.6 μs (NPR $=$ 4) and 6.6 μs (NPR $=$ 1.05).

Approximately 500 PIV image pairs were acquired per test case. Data from each image pair consisted of instantaneous streamwise, u, and cross-stream, v, velocities in the z and x directions respectively. The commercial software Insight v3.3 by TSI was used to process the images. A Fast Fourier Transform cross-correlation algorithm was used to extract the velocity vectors. Interrogation windows of 32 $\times$ 32 pixels with 75 per cent overlapping were employed in the processing. The size of the interrogation window was chosen to allow for a minimum of ten seeding particles per interrogation area and to allow for the maximum in-plane particle displacement to be less than one quarter of the size of the interrogation window. Inherent to PIV processing are the spurious vectors which,

on average, accounted for less than three per cent of the total. Images that generated velocity vector fields with spurious vectors of more than three standard deviations from the dataset mean were rejected (approximately five per cent). For those velocity vector fields that were not rejected, spurious vectors were filtered using a band-pass filter followed by a local median filter. The resulting empty spaces were filled with interpolated values from the surrounding area. The uncertainty in the measured velocity using PIV was estimated to be ± 3 per cent [21].

3.4 Laser Doppler velocimetry

LDV measurements were made using a Dantec FibreFlow system operating in backscatter mode. This consisted of a 4 W Lexel Model 95, water-cooled, argon-ion laser, a Dantec 60×41 transmitter with 60×24 fibre optic manipulators, Dantec 57N20 burst spectrum analyser, a Dantec 2D FiberFlow probe and a 1 m focal length lens with a $2\times$ beam expander. The lens and beam expander combination created a measurement volume of $0.15\ \text{mm} \times 4.2\ \text{mm} \times 0.15\ \text{mm}$. Bragg shifting by 40 MHz was used for directional discrimination. Alignment was completed using a 35 μm pinhole with a photovoltaic cell. Data processing included the filtering of any data outside three standard deviations from the mean. Mean and rms velocities were calculated using a weighted average technique. LDV data were acquired along a line joining the nozzle centrelines at heights above the ground of $z/D = 0.5$, $z/D = 1$ and $z/D = 2$. Each measurement point consisted of around 100 000 samples. The irregular time-spaced LDV data were resampled at regular intervals at twice the mean data rate using a nearest neighbour resampling technique. The resampled data were divided into segments of 2^{13} samples and processed using the Welch method and a Hanning window in order to reduce the spectral leakage. The uncertainty in the measured velocity using LDV was estimated to be ± 9 per cent [21].

4 Results

Results are presented for PIV and LDV measurements made under the following conditions.

- A nozzle spacing to diameter ratio, S/D, of seven.
- Nozzle height to diameter ratios, H/D, of 2.4, 4.4, 6.4 and 8.4.
- NPRs of 1.05, 2, 3, 3.25, 3.5, 3.75 and 4.
- Nozzle splay angles, α, of -15, -10, -5, 0, 5, 10 and 15 degrees.

4.1 Jet flow

The underexpanded impinging jet flow field can be divided into three main regions [22]: the free jet region, where the flow is primarily inviscid and contains the series of expansion and compression waves; the impingement region, which is characterised by strong gradients that alter significantly the local flow properties; the wall jet, which consists of a radial redirection of the jet flow after impingement.

4.1.1 Exit profiles

The fountain has been shown to be very sensitive to small variations in the generating jets, ground plane angle and even in the environment surrounding the experimental facilities [5]. Throughout the experiments the jets were generated by the same pair of nozzles, the ground plane was unvarying and the surrounding environment was similar. It was important, therefore, to check that the two jets had as near identical characteristics as possible. Figs. 4 and 5 show an example of LDV-measured velocity and turbulence intensity profiles respectively, $0.1D$ downstream of the nozzle exit plane; in this case at an NPR of three.

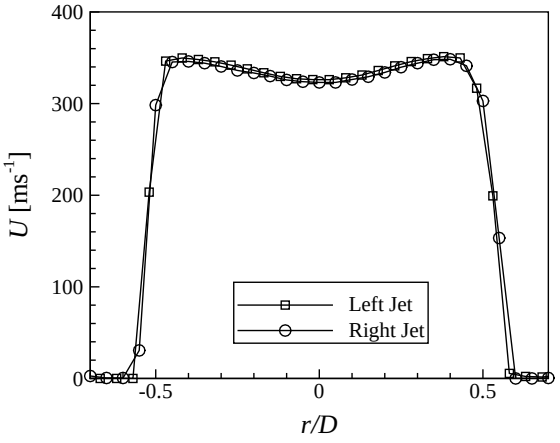

Fig. 4: LDV-measured velocity profiles $0.1D$ downstream of the nozzle exit plane (NPR = 3).

The velocity profiles (Fig. 4) are virtually identical with a maximum difference between the left and right jets of 0.8 per cent, which is well within the bounds

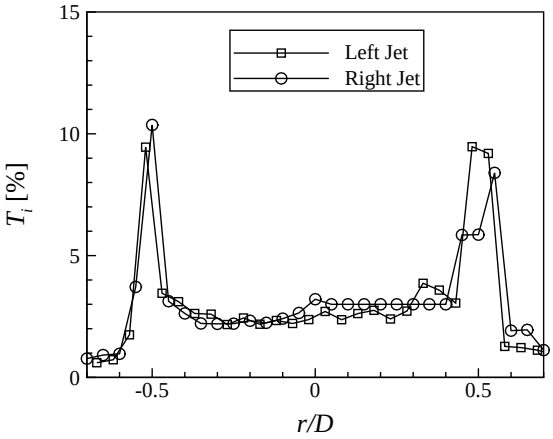

Fig. 5: LDV-measured turbulence intensity profiles $0.1\,D$ downstream of the nozzle exit plane (NPR $= 3$).

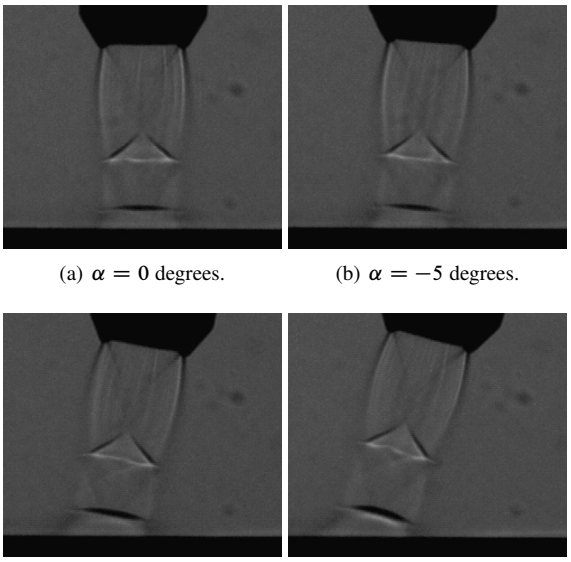

(a) $\alpha = 0$ degrees. (b) $\alpha = -5$ degrees.

(c) $\alpha = -10$ degrees. (d) $\alpha = -15$ degrees.

Fig. 6: Shadowgraph images showing impingement of the right-hand jet for four different nozzle splay angles ($H/D = 2.4$, NPR = 3.5).

of measurement uncertainty. The velocity profile exhibits a velocity deficit towards the centreline. This is characteristic of the curvature of the sonic line at the nozzle exit and typical of underexpanded jets issuing from convergent nozzles [23]. Peak turbulence intensity (Fig. 5) in the jet shear layer was in the region of ten per cent whilst on the jet centreline three per cent was typical. Both jets have turbulence intensity profiles which, within the limits of measurement uncertainty, are in agreement. Despite the care taken to ensure the jet flows were as near identical as possible, the fountain was found to lean relative to the vertical axis, although not consistently in one particular direction. In general, and with few exceptions, this phenomenon was shown to occur under the majority of the conditions tested.

4.1.2 Shock structure

When the nozzles are splayed, inwards or outwards, two distinct jet flow regions are formed, which are separated by the stand-off shock. Upstream of the stand-off shock the flow is axisymmetric and resembles that produced by a jet impinging normal to a plane surface; the stand-off shock remains parallel with the nozzle exit plane (Fig. 6). Downstream of the stand-off shock a non-axisymmetric flow region is identified.

4.1.3 Influence of the fountain

Figure 7 shows PIV-derived velocity magnitude contours superimposed onto a line integral convolution [24] plot at $H/D = 2.4$. The effect of the presence of the fountain is clearly visible in the entrainment process occurring on both sides of the jet. The left hand side (outer side) streamlines display a continuous entrainment of ambient air along the jet shear layer and wall jet. The right hand side (inner side) displays a different pattern. This is due to the presence of the fountain where the pressure is sub-atmospheric [5], inducing a higher velocity in the fountain-facing wall jet (inner side) and a thickening of the inner shear layer of the jet.

It is difficult to determine with absolute certainty the accuracy of the PIV measurements because detailed velocity field data are not available in the literature for this flow field. A comparison of PIV-derived Mach number data with a simple shadowgraph (Fig. 8) indicates, however, that the PIV has been able to capture the location of the important features of the underexpanded impinging jet.

4.2 Fountain

4.2.1 Flow visualization

The objective of this part of the study was to identify some of the oscillatory motions that exist in the fountain. It was found that increasing H/D increased the helical instability mode of the main jets, causing the fountain to oscillate more readily, resulting in a less well defined structure. Increasing S/D appeared to reduce the fountain oscillations and stabilise its stagnation point, however, wall jet development now oc-

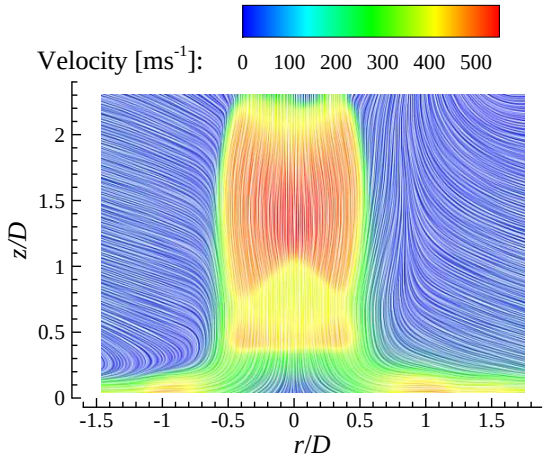

Fig. 7: PIV-derived contours of velocity magnitude with superimposed streamlines by the LIC technique for the left-hand jet ($S/D = 7$, $H/D = 2.4$, NPR $= 4$, $\alpha = 0°$).

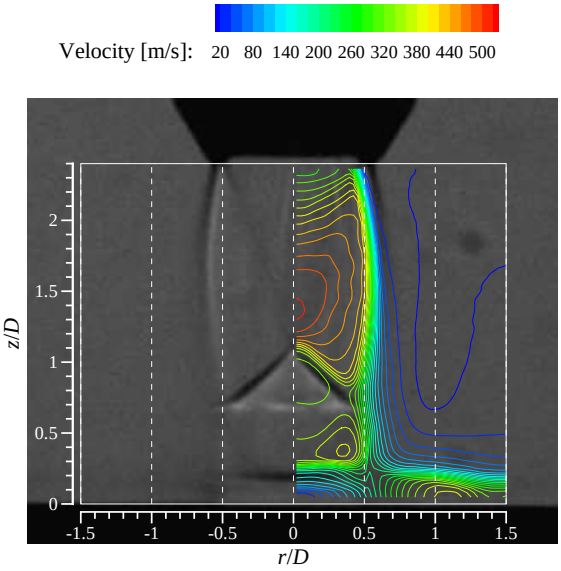

Fig. 8: PIV-derived contours of Mach number superimposed onto a shadowgraph image for the left-hand jet ($S/D = 7$, $H/D = 2.4$, NPR $= 4$, $\alpha = 0°$).

curred over a greater distance leading to the increased possibility of a wall jet momentum imbalance and a consequential time-mean inclination of the fountain. The main effect of changing nozzle splay angle was to change the fountain strength. An oscillatory flow pattern was observed under certain height and spacing combinations, driven by two rapidly-changing recirculation zones located between the fountain and the two main jets. Figure 9 shows a sequence of four images taken at a frame rate of 1 kHz. To improve the image resolution the camera field of view was limited to the fountain and the left-hand jet.

Figures 10 and 11 show two sequential instantaneous velocity magnitude contours superimposed onto a LIC plot at a non-dimensional nozzle height of $H/D = 4.4$. The images are separated temporally by 67 ms. The behaviour of the fountain flow is quite different from the jet flow in that the instantaneous velocity fields do not correlate well with the time-averaged one (Fig. 12) – indicating that it is a highly unsteady flow. This unsteadiness results from the collision of two wall jets that contain vortical structures and are themselves highly turbulent. The instantaneous velocity fields show a high degree of asymmetry, the presence of large-scale vortical structures and a stagnation region whose location has been observed to vary randomly. Although the instantaneous fountain flow is somewhat incoherent, it is clear from the images that it is inclined relative to the vertical. Through the observation of a sequence of these instantaneous velocity fields it appears that the fountain inclination is related to the strength and location of the dominant vortical structures. Unfortunately, the frame rate at which these data were acquired does not allow for the temporal resolution of these structures.

Figure 12 shows the mean velocity magnitude contours for $H/D = 4.4$ at an NPR of 3 and reveals two well-defined recirculation regions formed between the fountain and impinging jet flows. There is a recirculation zone to the left of the fountain, which is inclined to that side. A second recirculation zone is partially visible in the top right hand corner of this figure, however, it is the left-hand vortex which appears to dominate the flow. The fountain appears to be a bi-stable flow which, with symmetrical geometry and jet conditions, in the mean, would produce a fountain with no inclination. The time-averaged velocity contours were, therefore, quite surprising. The sample size of 500 is not large but should be sufficient to give a good representation of the mean. Further investigation showed the fountain inclination to be most likely dependent upon asymmetries in the geometry of the experimental rig. This was confirmed by swapping the nozzles over which, despite there being no measurable difference in geometry, changed the fountain inclination direction. These observations confirm the sensitivity of the fountain to small imbalances in the system [4], which has also been reported in other recent experiments on twin-jet fountain flows [18, 19].

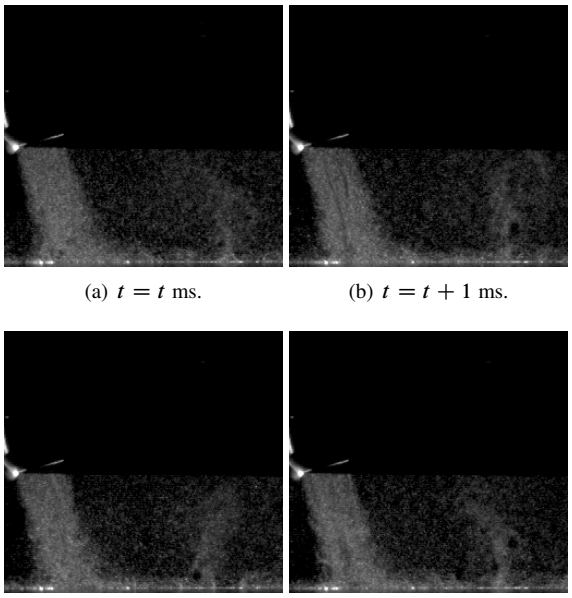

(a) $t = t$ ms. (b) $t = t + 1$ ms.

(c) $t = t + 2$ ms. (d) $t = t + 3$ ms.

Fig. 9: Typical 1 kHz flow visualization image sequence showing the left-hand jet flow and fountain ($S/D = 7$, $H/D = 2.4$, NPR = 1.05, $\alpha = -15°$).

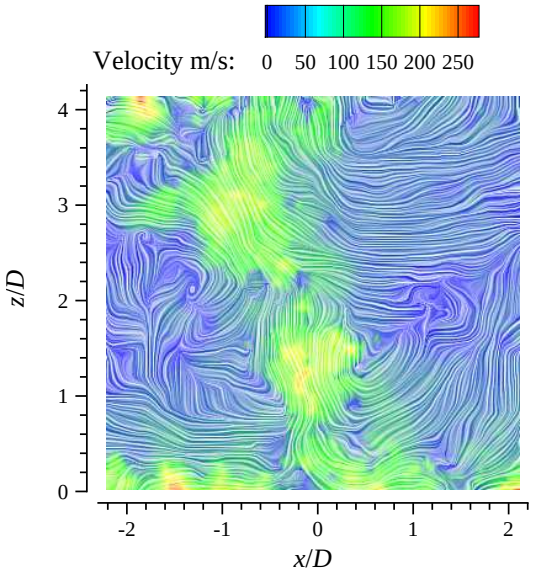

Fig. 10: Instantaneous velocity magnitude contours over LIC of the fountain flow ($S/D = 7$, $H/D = 4.4$, NPR $= 3$, $\alpha = 0°$).

4.2.2 Velocity decay

The effect of nozzle splay and pressure ratio on the time-mean peak vertical velocity in the fountain, $\hat{U}$, is shown in Fig. 13 for a nozzle height $H/D = 4.4$; other nozzle heights showed similar trends. ($\hat{U}$ is the highest measured vertical velocity in the fountain, whereas $U_{\max}$ is the highest measured vertical velocity in the fountain at a specific height.) For a fixed nozzle height, peak vertical velocity in the fountain was observed to be highly dependent upon the splay angle, with NPR having a secondary influence under choked nozzle conditions. Between NPR = 1.05 and NPR = 2, however, an increased upwash velocity was evident. The variation of peak fountain upwash velocity with NPR showed a strong dependence upon splay angle and a lesser dependence upon nozzle height. Increasing NPR for configurations with $\alpha = -15$ and -10 degrees resulted in the largest increase of peak vertical velocity. For a given NPR the largest peak upwash velocity was obtained with $\alpha = -15$ degrees and $H/D = 4.4$.

In order to further investigate the effect of parametric changes on the peak upwash velocity a method was sought by which the data could be non-dimensionalized. The ratio of peak vertical velocity in the fountain with a given nozzle height and splay angle to peak vertical velocity at the same nozzle height but with zero splay angle,

$$\frac{\hat{U}}{\hat{U}_{|\alpha=0°}} \tag{1}$$

was used to non-dimensionalize the velocity magnitude.

As nozzle splay angle is reduced the jets impinge closer to the geometric centre of the fountain; for certain configurations the jets may merge before impingement. This was observed to occur for the following configurations: $H/D = 6.4$, $\alpha = -15°$; $H/D = 8.4$, $\alpha = -15°$; $H/D = 8.4$, $\alpha = -10°$. Schach [25] showed that at impingement the stagnation point of an inviscid, incompressible, inclined jet is shifted $(D/2)\tan\alpha$ along the impingement plane towards the origin of inclination i.e. for the situation shown in Fig. 1 the stagnation point will be to the left of the extended centreline of the left-hand jet and to the right of the extended centreline of the right-hand jet.

For viscous conditions the change in non-dimensional distance between the stagnation points associated with the two jets is a function of the spreading rate of the jet itself as well as nozzle height, spacing and splay angle. Following the analysis of Bray [20] the jets have been assumed to have a half-angle, ϕ, of 4.6 degrees. The work of Schach [25] has, therefore, been extended here to include the effect of jet spreading and, with reference to the

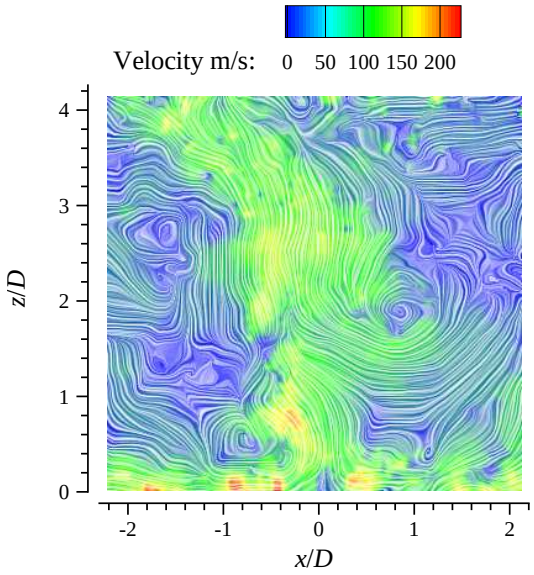

Fig. 11: Instantaneous velocity magnitude contours over LIC of the fountain flow 67 ms after Fig. 10 ($S/D = 7$, $H/D = 4.4$, NPR $= 3$, $\alpha = 0°$).

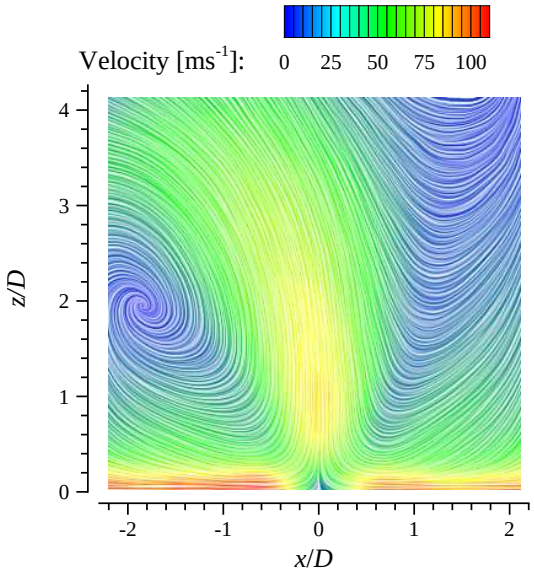

Fig. 12: Time-averaged velocity magnitude contours over LIC of the fountain flow ($S/D = 7$, $H/D = 4.4$, NPR $= 3$, $\alpha = 0°$).

geometric characteristics shown in Fig. 1, Equation 2 was derived.

$$\frac{L}{D} = \frac{S}{D} + \frac{2H\tan\alpha}{D} - \left[\left\{\frac{2H\tan\alpha}{D} + \cos\alpha\right\} - \left\{\left(\frac{2H}{D} - \sin\alpha\right)\tan(\alpha - \phi)\right\}\right]\sin\alpha \qquad (2)$$

where α is the splay angle and ϕ is the jet spreading half-angle. Equation 2 is presented in graphical form in Fig. 14. When $\phi = 0$ degrees the third term in Equation 2 simplifies to $\tan\alpha$, which is Schach's result in non-dimensional terms.

As well as affecting jet spacing at impingement, nozzle splay also affects the proportion of jet momentum flowing downstream away from the origin of the nozzle inclination (inwards towards the fountain in Fig. 1) to that travelling upstream (outwards in Fig. 1). Schach [25] gives the following equation

$$J = 1 - \frac{\pi/2 + \alpha}{\pi} + \frac{\sin(2(\pi/2 + \alpha))}{2\pi} \qquad (3)$$

for this ratio, which Rubel [26] has shown to be in good agreement with the experimental work of Taylor [27].

Figure 15 presents the ratio of non-dimensional peak vertical velocity in the fountain, $\hat{U}/\hat{U}_{|\alpha=0°}$, as a function of $J/(L/D)$ for NPR = 1.05. At such a low pressure ratio the effect of the shock cells observed at higher pressure ratios can be eliminated. The figure shows that, for the range of nozzle heights and splay angles considered, the data collapses quite well onto a single trend. A negative (inward) splay of the nozzles increases the non-dimensional peak fountain vertical velocity; decreasing the distance between the jets at impingement has the same effect.

Considering the configurations with underexpanded nozzle conditions the situation is not quite so straight forward. In general, the trend is very similar to that presented in Fig. 15, however, for some conditions there appears to be a strong NPR effect present. For $H/D = 4.4$ and a splay angle of -10° (labelled "A" in Fig. 16), $\hat{U}/\hat{U}_{|\alpha=0°}$ is independent of NPR whereas for $H/D = 2.4$ and a splay angle of -15° (labelled "B" in Fig. 16), $\hat{U}/\hat{U}_{|\alpha=0°}$ shows a clear dependence upon NPR. This inconsistency is most likely a consequence of the large changes in local jet velocity magnitude which can occur with relatively small changes in NPR [23].

The peak vertical velocity in the fountain appears, therefore, to be quite sensitive to the point within the shock cell at which impingement occurs. With positive splay angles the NPR dependence is less pronounced, which is most likely due to the reduced wall jet momentum flux towards the fountain formation region. Interestingly, with a nozzle splay angle of -5° peak fountain vertical velocity *decreases* with increas-

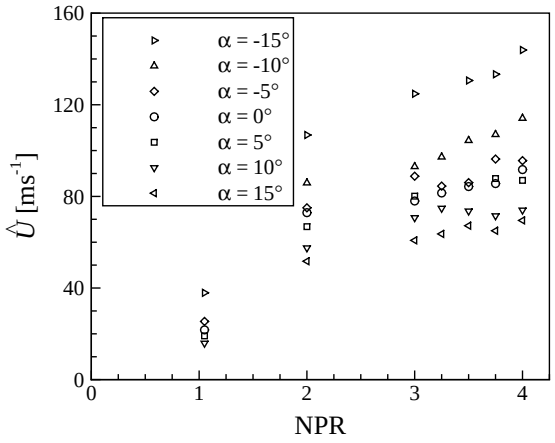

Fig. 13: PIV-measured mean peak vertical velocity, $\hat{U}$ in the fountain for a range of nozzle splay angles and pressure ratios ($S/D = 7$, $H/D = 4.4$).

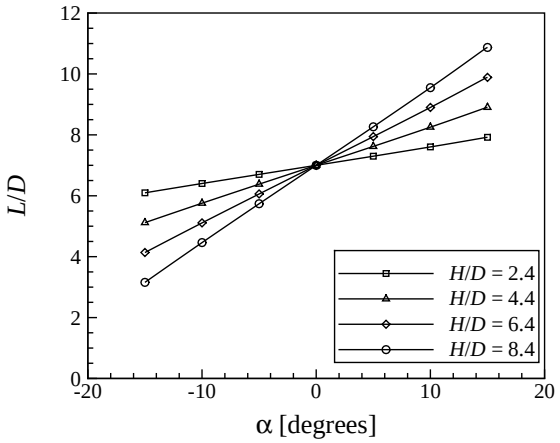

Fig. 14: Theoretical distance between the stagnation points of the jets at impingement.

ing NPR.

The local maximum vertical velocity in the fountain, $U_{\max}$, was found to vary approximately linearly with distance, z, normal to the ground plane. It is possible, therefore, to calculate the rate of decay of the local maximum vertical velocity, $\mathrm{d}\left(U_{\max}/U_j\right)/\mathrm{d}\left(z/D\right)$ and this is presented in non-dimensional terms in Figure 17. For a non-dimensional nozzle height, H/D, of 2.4 the data show that decay rate has a strong dependence upon NPR and that the variation in decay rate with nozzle splay angle is non-linear. There is a general trend, however, indicating that the rate of mean fountain vertical velocity decay decreases with increasing nozzle splay angle.

The NPR dependence is much reduced when the nozzle height is increased to $H/D = 4.4$, however, the non-linear variation of decay rate with nozzle splay angle remains. Increasing nozzle height further to $H/D = 6.4$ and $H/D = 8.4$ reveals a much more linear variation of mean fountain vertical velocity decay rate with nozzle splay angle.

4.2.3 Spreading rate

Values of fountain half-width, $x_{0.5}$, were extracted from the mean velocity data for all nozzle configurations. The half-width was only calculated where the condition $U/U_{\max} < 0.5$ was satisfied on both sides of the fountain velocity profile. Fountain half-width was found to vary quite linearly with height above the ground for all the tested conditions. Negative (inward) splayed nozzle configurations presented the smallest values of fountain half-width, demonstrating that the fountain becomes narrower with decreasing splay angle. This qualitative variation of fountain half-width with splay angle was consistently observed for each combination of nozzle height and pressure ratio.

The fountain's growth rate (or spreading rate), the variation of $x_{0.5}$ with distance from the impingement plane, can be represented by

$$\frac{x_{0.5}}{D} = a_1\left(\frac{z}{D}\right) + a_2 \qquad (4)$$

where a_1 is the growth rate of the fountain half-width, and a_2 is the half-width at $z = 0$. Although at the fountain base the half-width is approximately constant for a given splay angle, its variation with increasing height above the ground, defined by the growth rate, $\mathrm{d}x_{0.5}/\mathrm{d}z$, is quantitatively different across the test matrix; an example is shown in Fig. 18. It was found that with decreasing nozzle height, varying splay angle and NPR induced larger variations in the fountain growth rate.

At $H/D = 2.4$ the average variation in spreading rate (relative to the parallel nozzle configuration) with splay angle is 68 per cent, whereas the average variation with nozzle pressure ratio is 14 per cent. At $H/D = 8.4$ these values reduce to 17 per cent and 6 per cent respectively. The effect of increasing nozzle splay angle is noticeably different at different nozzle heights. At $H/D = 2.4$ a decrease in splay angle (for $\alpha < 0°$) results in a decrease in the fountain growth rate that approximately has the same magnitude as the equivalent increase in nozzle splay angle (for $\alpha > 0°$). With increasing nozzle height, increasing nozzle splay angle (for $\alpha > 0°$) tends to increase the fountain

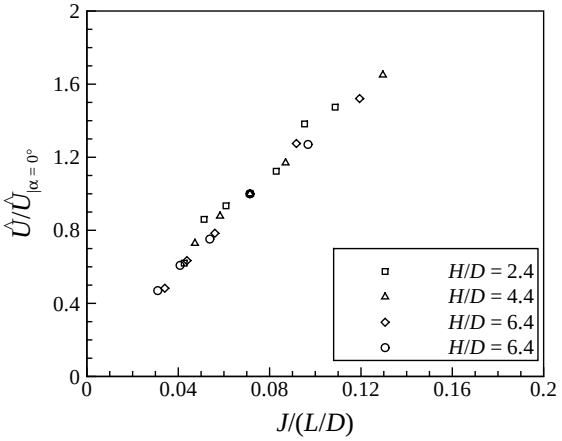

Fig. 15: Non-dimensional peak fountain vertical velocity as a function of $J/(L/D)$ ($S/D = 7$, NPR = 1.05).

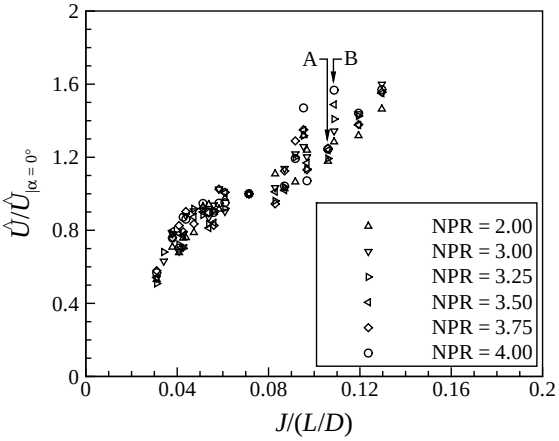

Fig. 16: Non-dimensional peak fountain vertical velocity as a function of $J/(L/D)$ for various NPRs ($S/D = 7$).

growth rate. On average, increasing nozzle splay angle from $\alpha = 0°$ to $\alpha = 15°$ results in a 26 per cent increase in the fountain growth rate at $H/D = 2.4$. The same variation in splay angle at $H/D = 8.4$ only results in a 3 per cent increase in fountain growth rate.

4.2.4 Momentum flux ratio

Vertical velocity profiles, when non-dimensionalized with the local maximum mean fountain upwash velocity, $U_{\max}$, and fountain half width, $x_{0.5}$, were self-similar for all nozzle heights and pressure ratios under investigation. With splayed nozzle configurations, profiles of mean vertical velocity were also found to exhibit self-similarity and this behaviour occurred independent of nozzle height, splay angle and pressure ratio. An example is shown in Fig. 19 for $z/D = 1.5$.

Momentum flux ratio was calculated using the same method as that described in Reference [28]. Generally it was found that the inclusion of nozzle splay did not alter significantly the distribution of fountain momentum flux ratio, $\lambda_{\dot{M}}$, relative to the equivalent parallel configuration. At a nozzle height of $H/D = 4.4$ the position of maximum momentum flux ratio occurred further downstream in the fountain (higher z/D) for configurations with negative nozzle splay angles. For configurations with negative nozzle splay angle the position of maximum momentum flux ratio occurred at $z/D \approx 3.25$, whereas for configurations with parallel and positive nozzle splay angles the position of maximum momentum flux ratio was found to occur at $z/D \approx 2.5$.

At $H/D = 6.4$ and $H/D = 8.4$ there was a strong similarity between the distributions of momentum flux ratio across the range of nozzle splay angles and pressure ratios; Fig. 20 shows the case for NPR = 3. In general the position of maximum momentum flux ratio occurred at $z/D \approx 2.8$ ($H/D = 6.4$) and $z/D \approx 3.0$ ($H/D = 8.4$).

4.2.5 Power spectral density

The increased level of spreading observed in the fountain when compared to normal jet development may, in part, be due to the oscillation of the flow, resulting in a fountain that appears to spread more than its instantaneous structure would suggest. Further study would be needed to establish whether this is an acoustically-induced phenomenon of the type reported by Krothapalli et al. [29]. It is evident that the fountain upwash is unsteady, however the data rate of the PIV system did not permit the quantification of transient features of this flow region. The high data rate LDV measurements address this issue, capturing the smaller-scale high-frequency components of the upwash oscillation. The data gathered showed that the majority of the horizontal turbulent energy in the upwash is contained within the first 600 Hz of the frequency spectra, decaying with further increases in frequency: an example is shown in Fig. 21. The slope of the decay of horizontal turbulent energy followed the -5/3 spectral law [30]. For $H/D = 2.4$, 6.4 and 8.4 the spectra showed a similar pattern, with increasing horizontal energy for increasing NPR and decreasing z/D, however, at $H/D = 4.4$ the frequency distribution of the horizontal energy displayed a pattern not observed at other

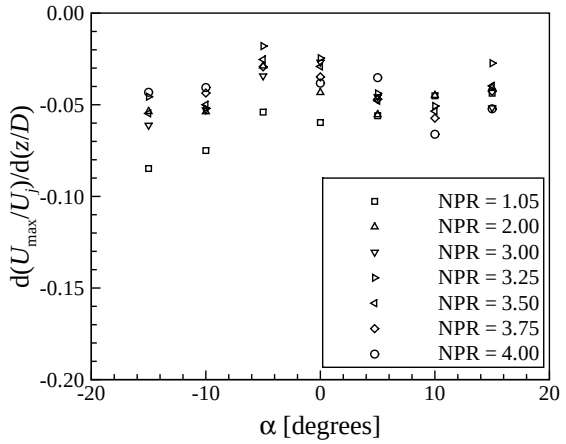

Fig. 17: PIV-derived mean fountain vertical velocity decay rate ($S/D = 7$, $H/D = 2.4$).

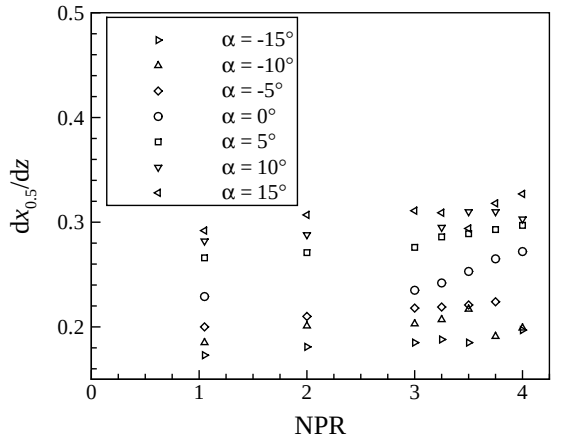

Fig. 18: PIV-derived growth rate of the fountain half-width, $\mathrm{d}x_{0.5}/\mathrm{d}z$ ($S/D = 7$, $H/D = 2.4$).

nozzle heights. At this nozzle height and for underexpanded jet conditions only, the power spectral density (PSD) distribution had a distinct peak. The frequency at which the peak occurred was observed to increase with increasing NPR; at 180 Hz and 240 Hz for NPR = 2 and NPR = 3 respectively. At NPR = 4 no distinct peak was observed, although a broadband 'hump' was identified at 300 Hz for $z/D = 1$ and $z/D = 2$. The fact that the frequency of the peaks does not change with varying horizontal position (Fig. 22) implies that under the particular test conditions the distribution of horizontal energy is dominated by large-scale structures (with dimensions of at least $0.4D$) rather than by the small scales of turbulence.

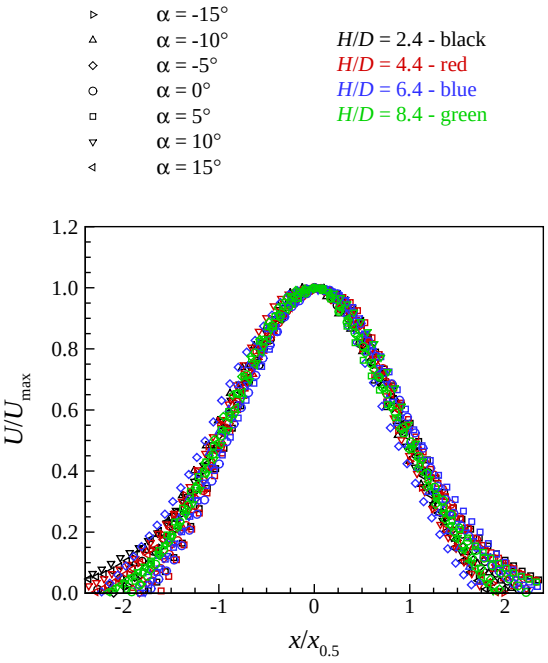

Fig. 19: PIV-measured non-dimensional mean vertical velocity profiles ($S/D = 7$, $z/D = 1.5$, NPR = 2).

5 Conclusions

An investigation has been conducted on the fountain flowfield formed by the impingement of two high-speed, turbulent, compressible jets. Mean fountain characteristics were acquired for nozzle pressure ratios of between 1.05 and 4, nozzle height-to-diameter ratios of between 2.4 and 8.4, nozzle splay angles of between ± 15 degrees and a nozzle spacing-to-diameter ratio of seven. Shadowgraph images of the jet impingement region showed that the stand-off shock remains parallel to the nozzle exit plane even when the jet is inclined to the impingement plane by up to 15 degrees. It was shown that for a low nozzle pressure ratio (1.05) there was good correlation between, the product of the jet momentum carried towards the fountain formation region and the lateral separation of the jet stagnation points, and the ratio of peak vertical velocity in the fountain. For underexpanded pressure ratios the correlation still exists, however, there was more scatter in the data. This was thought to be due to changes in the shock cell structure caused, for example by small changes in NPR, having a strong influence on the jet velocity at impingement. The rate of decay of maximum vertical velocity in the fountain was shown to have a strong dependence on nozzle pressure ratio and that the variation in decay rate with nozzle splay angle

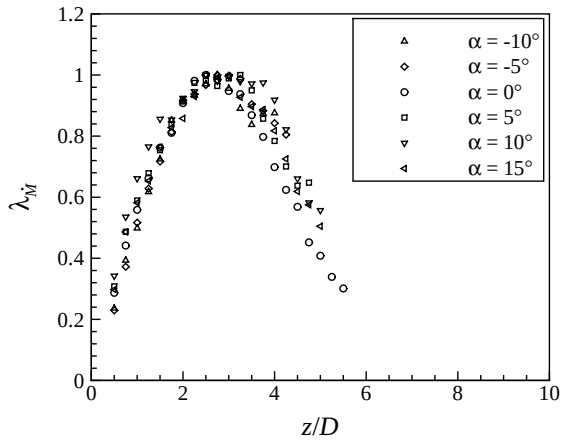

Fig. 20: PIV-derived vertical distribution of momentum flux ratio, $\lambda_{\dot{M}}$, through the fountain (S/D = 7, H/D = 6.4, NPR = 3).

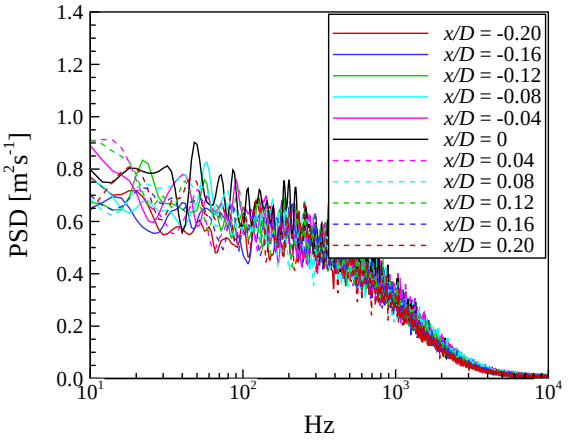

Fig. 21: LDV-derived power spectral density peaks for varying horizontal position (S/D = 7, H/D = 2.4, z/D = 1, NPR = 2).

is, at the lower nozzle heights, non-linear with nozzle splay angle. Fountain spreading rate was observed to have a strong dependence upon nozzle splay angle at low nozzle heights but a negligible dependence once nozzle height had reached 8.4 diameters. In general it was found that the inclusion of nozzle splay did not alter significantly the distribution of fountain momentum flux ratio relative to the equivalent parallel configuration. The fountain spectral measurements showed a distinct frequency of horizontal oscillations. This frequency was only observed in the spectra with under-expanded jets and for a nozzle height-to-diameter ratio of 4.4 and correlated with increased spreading rates of the fountain.

Acknowledgements

This work was partly funded by the Engineering and Physical Sciences Research Council under grant GR/R42894/01 and their support is gratefully acknowledged.

References

[1] Kuhn, R. E., Margason, R. J., and Curtis, P., *Jet Induced Effects: The Aerodynamics of Jet and Fan Powered V/STOL Aircraft in Hover and Transition*, Vol. 217, AIAA, Reston, VA 20191-4344, 2006.

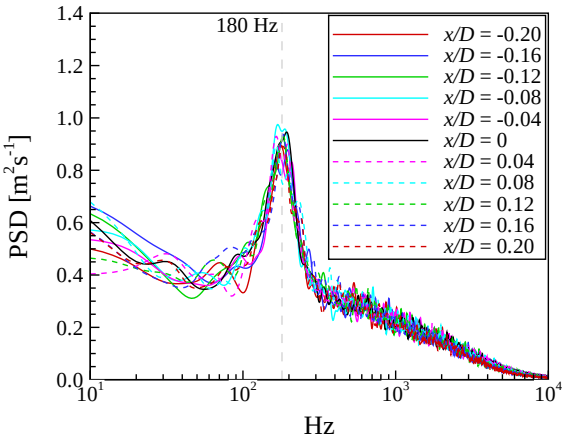

Fig. 22: LDV-derived power spectral density peaks for varying horizontal position (S/D = 7, H/D = 4.4, z/D = 1, NPR = 2).

[2] Margason, R. J., "Review of Propulsion-induced Effects on Aerodynamics of Jet/STOL Aircraft," Technical Note D-5617, NASA, 1970.

[3] Saddington, A. J., Cabrita, P. M., and Knowles, K., "Large-scale Instabilities in a STOVL Upwash Fountain," *Engineering Turbulence Modelling and Experiments 6*, edited by W. Rodi and M. Mulas, Elsevier Science Ltd., Oxford, UK, 2005, pp. 667–676, ISBN: 0 08 044544 6.

[4] Skifstad, J. G., "Aerodynamics of Jets Pertinent to VTOL Aircraft," *Journal of Aircraft*, Vol. 7, No. 3, 1970, pp. 193–204.

[5] Abbott, W. A. and White, D. R., "The Effect of Nozzle Pressure Ratio on the Fountain Formed Between Two Impinging Jets," Technical Memorandum P1166, RAE, 1989.

[6] Hall, G. R. and Rogers, K. H., "Recirculation Effects Produced by a Pair of Heated Jets Impinging on a Ground Plane," Contractor Report CR-1307, NASA, 1969.

[7] Gilbert, B. L., "Turbulence Measurements in a Radial Upwash," *AIAA Journal*, Vol. 27, No. 1, January 1989, pp. 44–51.

[8] Barata, J. M. M., "Fountain Flows Produced by Multi-jet Impingement on a Ground Plane," *AIAA Journal of Aircraft*, Vol. 30, No. 1, 1993, pp. 50–56.

[9] Behrouzi, P. and McGuirk, J. J., "Experimental Data for CFD Validation of Impinging Jets in Cross-flow with Application to ASTOVL Flow Problems," *AGARD Conference Proceedings CP-534, Fluid Dynamics Panel Symposium*, Winchester, UK, 19-22 April 1993.

[10] Siclari, M. J., Hill, W. G., and Jenkins, R. C., "Stagnation Line and Upwash Formation of Two Impinging Jets," *AIAA Journal*, Vol. 19, No. 10, October 1981, pp. 1286–1293.

[11] Wohllebe, F. A. and Siclari, M. J., "Fountain and Upwash Flowfields of Multijet Arrangements," *Journal of Aircraft*, Vol. 15, No. 8, August 1978, pp. 468–473.

[12] Saripalli, K. R., "Visualization of Multijet Impingement Flow," *AIAA Journal*, Vol. 21, No. 4, April 1983, pp. 483–484.

[13] Kibens, V., Saripalli, K. R., Wlezien, R. W., and Kegelman, J. T., "Unsteady Features of Jets in Lift and Cruise Modes for VTOL Aircraft," *International Powered Lift Conference and Exhibit*, Santa Clara, CA, USA, 7-10 December 1987, pp. 543–552, Paper no. 872359.

[14] Cabrita, P. M., Saddington, A. J., and Knowles, K., "Unsteady Features of Twin-jet STOVL Ground Effects," *International Powered Lift Conference and Exhibit*, Williamsburg, VA, USA, 5-7 November 2002, Paper no. 2002-6014.

[15] Childs, R. E. and Nixon, D., "Turbulence and Fluid/Acoustic Interaction in Impinging Jets," *International Powered Lift Conference and Exhibit*, Santa Clara, CA, USA, 7-10 December 1987, pp. 447–458, Paper no. 872345.

[16] Knowles, K., Wilson, M. J., and Bray, D., "Unsteady Pressures Under Impinging Jets in Crossflows," *AIAA Journal*, Vol. 31, No. 12, 1993, pp. 2374–2375.

[17] Kotansky, D. R. and Glaze, L. W., "The Effects of Ground Wall-jet Characteristics on Fountain Upwash Flow Formation and Development," *14th AIAA Fluid and Plasma Dynamics Conference*, Palo Alto, CA, USA, 23-25 June 1981, Paper no. 81-1294.

[18] El-Okda, Y. and Telionis, D. P., "Experimental Investigation of Twin Jet Impinging on the Ground With and Without a Free Stream," *International Powered Lift Conference and Exhibit*, Williamsburg, VA, USA, 5-7 November 2002, Paper no. 2002-5976.

[19] Elavarasan, R., Venkatakrishnan, L., Krothapalli, A., and Lourenço, L., "Supersonic Twin Impinging Jets," *38th Aerospace Sciences Meeting and Exhibit*, Reno, NV, USA, 10-13 January 2000, Paper no. 2000-0812.

[20] Bray, D., *Jets in Cross-flow and Ground Effect*, PhD thesis, Cranfield Institute of Technology, Shrivenham, UK, 1992.

[21] Cabrita, P. M., *Steady and Unsteady Features of Twin-Jet STOVL Ground Effects*, PhD thesis, Cranfield University, Shrivenham, UK, 2006.

[22] Donaldson, C. D. and Snedeker, R. S., "A Study of Free Jet Impingement. Part 1. Mean Properties of Free and Impinging Jets," *Journal of Fluid Mechanics*, Vol. 45, No. 2, 1971, pp. 281–319.

[23] Saddington, A. J., Lawson, N. J., and Knowles, K., "An Experimental and Numerical Investigation of Under-expanded Turbulent Jets," *The Aeronautical Journal*, Vol. 108, No. 1081, March 2004, pp. 145–152.

[24] Knowles, R. D., Finnis, M. V., Saddington, A. J., and Knowles, K., "Planar Visualization of Vortical Flows," *IMechE Part G: Journal of Aerospace Engineering — Special Issue on Integrating CFD and Experiments in Aerodynamics*, Vol. 220, No. 6, 2006, pp. 619–627.

[25] Schach, W., "Umlenkungeinesfreien Flussigkeitsstrahles an einer ebenen Platte (The Deflection of a Free Liquid Jet on a Flat Plane)," *Ingenieur-Archiv*, Vol. 5, 1934, pp. 245–265.

[26] Rubel, A., "Oblique Impingement of a Round Jet on a Plane Surface," *AIAA Journal*, Vol. 20, No. 12, 1982, pp. 1756–1758.

[27] Taylor, G., "Oblique Impact of a Jet on a Plane Surface," *Philosophical Transactions of the Royal Society*, Vol. 260A, 1966, pp. 96–100.

[28] Saddington, A. J., Knowles, K., and Cabrita, P. M., "Flow Measurements in a Short Take-Off, Vertical Landing Fountain: Parallel Jets," *Journal of Aircraft*, Vol. 45, No. 5, 2008, pp. 1736–1743.

[29] Krothapalli, A., Rajakuperan, E., Alvi, F. S., and Lourenço, L., "Flow Field and Noise Characteristics of a Supersonic Impinging Jet," *Journal of Fluid Mechanics*, Vol. 392, August 1999, pp. 155–181.

[30] Tennekes, H. and Lumley, J. L., *A First Course in Turbulence*, MIT Press, Cambridge, MA, USA, 1972.

Cranfield University

CERES Research Repository **https://dspace.lib.cranfield.ac.uk/**

Cranfield Defence and Security Staff publications (CDS)

On the Characteristics of a Twin-Jet STOVL Fountain

Saddington, Alistair J.

2015-03-03

Saddington AJ, Knowles K, Cabrita PM. (2009) On the characteristics of a twin-jet STOVL fountain. The Aeronautical Journal. Volume 113, Issue 1140, February 2009, pp. 139-148.
http://dspace.lib.cranfield.ac.uk/handle/1826/9149
Downloaded from CERES Research Repository, Cranfield University